

**Spin-orbit interaction of light: When twisted light meets twisted metasurfaces**Wenshuai Zhang , Yongsheng Wang, Dingyu Xu, and Hailu Luo \**Laboratory for Spin Photonics, School of Physics and Electronics, Hunan University, Changsha 410082, China*

(Received 21 November 2022; accepted 29 March 2023; published 7 April 2023)

Singular optics and metamaterials are both fascinating branches of modern optics. While the twist of vortex beams in phase and polarization leads to singularities, the twist of metasurfaces also leads to extraordinary properties in both optics and electronics. Here we present the spin-orbit interaction of a vortex beam reflected on twisted few-layer hyperbolic metasurfaces. As a result, the spatial Imbert-Fedorov (IF) shift and photonic spin Hall effect (PSHE) shift are investigated. We find that the spatial IF shift versus twist angle is symmetrical about the  $l = 0$  shift and it is symmetrical about the origin for opposite twist angle with opposite topological charge. In addition, the PSHE shift versus twist angle is also symmetrical about the  $l = 0$  shift. The shifts are enhanced with increasing topological charge and show a pretty different dependence on the twist angle when the incident beam is in different polarization state. These findings provide a different perspective for further investigations of twisted light and twisted metasurfaces.

DOI: [10.1103/PhysRevA.107.043502](https://doi.org/10.1103/PhysRevA.107.043502)**I. INTRODUCTION**

In the field of interaction between light and matter, three important aspects may come into view: The polarization of light, the optical wave front of light, and the structure of materials [1,2]. The polarization and wave fronts of light can be evident through studies of the vortex beam. The optical vortices of the vortex beam are characterized by the topological charge which is equal to the number of wave-front branches near the singular point [3,4]. Since the vortex beam carries intrinsic orbit angular momentum (OAM) that comes from the screw phase dislocation aligned with the optical axis, it had caught plenty of attention and been explored in fields including optics, electronics, and acoustics [5–10]. General methods generating vortex beams include the spatial light modulator, cylindrical lens, spiral split, and metasurfaces [11–15]. With vortex beams being widely applied in optical communications, image processing, material processing, and the manipulation of light, the method of manipulating optical properties such as topological charge [16], polarization, and the phase of the vortex beam is of great importance [17–21]. Therefore, shifts of the beam with OAM have been a focused topic [22,23]. Within the spin-orbit interaction of vortex beams [24], Goos-Hänchen shifts and Imbert-Fedorov shifts of the vortex beam were investigated [25–27], as well as the spin Hall effect of the vortex beam [28–30]. In addition, the Doppler shifts of the beam-carrying OAM were investigated [31,32]. Generally, the shifts were considered for the light beam reflected on homogeneous materials [33,34] or transferring in free space [24,29].

In recent years, stacked two-dimensional (2D) materials with a relative twist angle between each layer have become a focal point [35–38]. For example, the photonic spin Hall effect (PSHE) of twisted bilayer graphene has shown a unique

dependence on the twist angle and frequency because of the moiré pattern, which comes from the twist and interlayer interaction of graphene layers [39]. In addition to the 2D atomic crystals, metasurface, an artificial 2D nanostructured material [40,41], exhibits extraordinary properties in both optics and electronics, showing new features with twisted structures [42–48]. When the metasurfaces are stacked in few-layer structures instead of a monolayer, the applicability of metasurfaces is then greatly improved [49–51]. The few-layer structure of metasurfaces is able to provide more degrees of freedom for the manipulation of the polarization state and phase of light, which makes it obtain an ultrasensitive optical response to the twist between each layer as well as the interlayer refractive index.

Here, we investigate the spin-orbit interaction between the vortex beam and twisted hyperbolic metasurfaces, which manifests as a spatial Imbert-Fedorov (IF) shift and PSHE shift. We propose a simple model to describe the conductivity and reflection coefficients of the twisted metasurfaces. The results show that the shifts are dependent on the twist angle and symmetrical about the  $l = 0$  shift for opposite topological charge. As examples, twisted bilayer and trilayer metasurfaces are taken into consideration in the demonstrations. The shifts are enhanced near the Brewster angle and are within the wavelength range, which can be detected in current experiment capabilities. Also, for a fixed incident angle and frequency, the shifts are closely related to the twist structure and robust for complex backgrounds. The interaction between twisted light and twisted metasurface leads to the unique symmetry properties of IF shifts and PSHE shifts, which holds great potential in the application of vortex beams and many other twisted 2D materials.

**II. THEORETICAL MODELS**

We begin by analyzing the interaction system depicted in Fig. 1(a). A vortex beam of topological charge  $l$  and frequency

\*hailuluo@hnu.edu.cn

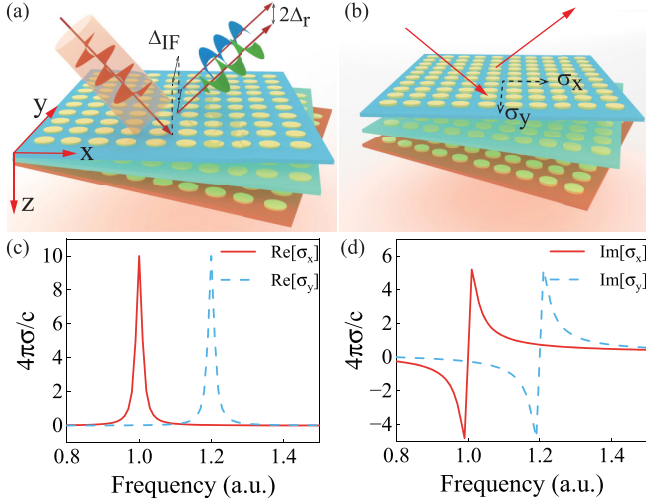


FIG. 1. (a) Schematic representation of the vortex beam reflected at the twisted metasurfaces with the corresponding spatial IF shift and PSHE split. (b) Front-view-rendered image of the twisted metasurfaces. The direction of the conductivities are also shown. (c,d) Real part and imaginary part of the conductivity along ( $\sigma_x$ ) and across ( $\sigma_y$ ) the main axis of the metasurface, respectively.

$\omega$  propagating in a vacuum impinges at incident angle  $\theta_i$  on the twisted metasurfaces. For convenience, the background and interlayer materials are assumed to be free space, but the asymmetric refractive index of the backgrounds can be also captured by generalizing the formulations. The angular spectrum of the incident beam presented in the local coordinate system can be expressed as [26]

$$\begin{aligned} \tilde{\mathbf{E}}_i &= [f_p \hat{\mathbf{x}}_i + f_s \hat{\mathbf{y}}_i] \tilde{u}_i, \\ \tilde{u}_i &= \frac{C_l w_0}{2} \left[ \frac{w_0 (-ik_{ix} + \text{sgn}[l]k_{iy})}{\sqrt{2}} \right]^{|l|} \\ &\quad \times \exp \left[ -\frac{w_0^2 (k_{ix}^2 + k_{iy}^2)}{4} \right], \end{aligned} \quad (1)$$

where  $\tilde{u}_i$  is the angular spectrum of the vortex beam,  $C_l = \sqrt{2/(\pi|l|!)}$  is the normalization constant, and  $w_0$  is the beam waist. Here, the polarization state of the incident beam is determined by the complex unit vector  $\hat{\mathbf{f}} = f_p \hat{\mathbf{x}}_i + f_s e^{i\xi} \hat{\mathbf{y}}_i$  where  $f_p$  and  $f_s$  are real-valued amplitudes corresponding to the vertical and horizontal polarization states, respectively, where  $\xi$  is the relative phase shift between these two components.

The expression of the reflected angular spectrum of the incident beam can be obtained by enforcing the reflection law and Fresnel's equations for each component of the incident beam, as well as the paraxial approximation. Here, the reflection coefficients and the reflected beam components can be written as [52]

$$\begin{bmatrix} \tilde{\mathbf{E}}_r^p \\ \tilde{\mathbf{E}}_r^s \end{bmatrix} = \begin{bmatrix} r_{pp} & r_{ps} \\ r_{sp} & r_{ss} \end{bmatrix} \begin{bmatrix} \tilde{\mathbf{E}}_i^p \\ \tilde{\mathbf{E}}_i^s \end{bmatrix}, \quad (2)$$

where we introduce boundary conditions  $k_{rx} = -k_{ix}$  and  $k_{ry} = k_{iy}$ . In addition, the Taylor series expansion based arbitrary angular spectrum components is also included.

Therefore, the reflected beam can be easily obtained as

$$\begin{aligned} \tilde{\mathbf{E}}_r &= f_p \left[ r_{pp} - \frac{\partial r_{pp}}{\partial \theta_i} \frac{k_{rx}}{k} + \frac{(r_{sp} - r_{ps})k_{ry}}{k} \cot \theta_i \right] \tilde{u}_r \hat{\mathbf{x}}_r \\ &\quad + f_s \left[ r_{ps} - \frac{\partial r_{ps}}{\partial \theta_i} \frac{k_{rx}}{k} + \frac{(r_{pp} + r_{ss})k_{ry}}{k} \cot \theta_i \right] \tilde{u}_r \hat{\mathbf{x}}_r \\ &\quad + f_p \left[ r_{sp} - \frac{\partial r_{sp}}{\partial \theta_i} \frac{k_{rx}}{k} - \frac{(r_{pp} + r_{ss})k_{ry}}{k} \cot \theta_i \right] \tilde{u}_r \hat{\mathbf{y}}_r \\ &\quad + f_s \left[ r_{ss} - \frac{\partial r_{ss}}{\partial \theta_i} \frac{k_{rx}}{k} + \frac{(r_{sp} - r_{ps})k_{ry}}{k} \cot \theta_i \right] \tilde{u}_r \hat{\mathbf{y}}_r. \end{aligned} \quad (3)$$

The shifts for different circularly polarized components of the reflected beam can be obtained by calculating the centroid of the intensity distribution. The total shift can be expressed in terms of the spatial IF shift of the entire beam and the PSHE shift of different polarization states as

$$\Delta_r^\pm = \Delta_{IF} \pm \Delta_{\text{PSHE}}^\pm. \quad (4)$$

Here, the spatial IF shift  $\Delta_{IF}$  can be obtained by [25,34]

$$\Delta_{IF} = \frac{\iint \partial_{k_{ry}} |\tilde{\mathbf{E}}_r|^2 dk_{rx} dk_{ry}}{\iint |\tilde{\mathbf{E}}_r|^2 dk_{rx} dk_{ry}}. \quad (5)$$

Then, for linearly polarized incident beams  $f_p = 1$  and  $f_s = 0$ , the spatial IF shift can be simplified to

$$\Delta_{IF} = \frac{-l \text{Re}[\alpha_1] + \text{Im}[\alpha_2]}{k(|r_{pp}|^2 + |r_{sp}|^2)}, \quad (6)$$

where

$$\begin{aligned} \alpha_1 &= r_{pp} \frac{\partial r_{pp}^*}{\partial \theta_i} + r_{sp} \frac{\partial r_{sp}^*}{\partial \theta_i}, \\ \alpha_2 &= r_{pp} (r_{ps}^* - r_{sp}^*) \cot \theta_i + r_{sp} (r_{pp}^* + r_{ss}^*) \cot \theta_i. \end{aligned} \quad (7)$$

With the same method, the shift  $\Delta_r^\pm$  for the right- and left-circular polarized reflected beams can be obtained by

$$\Delta_r^\pm = \frac{\iint \partial_{k_{ry}} |\tilde{\mathbf{E}}_r^\pm|^2 dk_{rx} dk_{ry}}{\iint |\tilde{\mathbf{E}}_r^\pm|^2 dk_{rx} dk_{ry}}. \quad (8)$$

Here,  $\tilde{\mathbf{E}}_r^+$  and  $\tilde{\mathbf{E}}_r^-$  represent the right-circular and left-circular polarized reflected beams, respectively. Then the PSHE shift can be obtained as

$$\Delta_{\text{PSHE}}^\pm = \Delta_r^\pm \mp \Delta_{IF}, \quad (9)$$

where

$$\Delta_r^\pm = \frac{l \text{Re}[\beta_1^\pm \beta_3^{\pm*}] - \text{Im}[\beta_1^{\pm*} \beta_2^\pm]}{|\beta_1^\pm|^2}, \quad (10)$$

and

$$\begin{aligned} \beta_1^\pm &= r_{pp} \mp i r_{sp}, \\ \beta_2^\pm &= -\frac{(r_{ps} - r_{sp}) \cot \theta_i}{k} \pm i \frac{(r_{pp} + r_{ss}) \cot \theta_i}{k}, \\ \beta_3^\pm &= \frac{1}{k} \left( -\frac{\partial r_{pp}}{\partial \theta_i} \pm i \frac{\partial r_{sp}}{\partial \theta_i} \right). \end{aligned} \quad (11)$$

To numerically evaluate the spatial IF shift and PSHE shift arising from the reflection on the twisted metasurfaces, one needs to obtain the reflection coefficients of the twisted metasurfaces. Making use of the generalized transfer matrix formalism for arbitrary anisotropic 2D layers, the reflection coefficients of the twisted metasurfaces can be obtained by components of the transfer matrix.

The reflection coefficients are closely related to the conductivity tensor  $\hat{\sigma}$  of each hyperbolic metasurface layer shown in Fig. 1(b), which consists of a 2D uniaxial plasmonic array. Each single-layer hyperbolic metasurface shown in the figure without any twist can be expressed as [53]

$$\hat{\sigma} = \begin{pmatrix} \sigma_x & 0 \\ 0 & \sigma_y \end{pmatrix}. \quad (12)$$

The conductivity describes the resonant interaction between individual scatterers in the plasmonic layer. It can be obtained in local response approximations with a Lorentzian form as

$$\sigma_{x,y} = \sigma_{x,y}^{\infty} + \frac{A_{x,y}i\omega}{\omega^2 - \Omega_{x,y}^2 + i\omega\gamma_{x,y}}, \quad (13)$$

where  $\Omega_{x,y}$  and  $\gamma_{x,y}$  are the resonant frequencies and corresponding bandwidths along and across the main axis,  $A_{x,y}$  are the corresponding oscillator strengths, and  $\sigma_{x,y}^{\infty}$  are the responding background conductivities caused by a nondipole response or finite thickness of a plasmonic layer. The dimensionless conductivity owing to the realistic parameters that correspond to a thin plasmonic array is shown in Fig. 1(b). The parameter settings of the plasmonic metasurface in arbitrary units (a.u.) are  $\sigma_{x,y}^{\infty} = 0.2i$ ,  $A_{x,y} = 0.2$ ,  $\Omega_x = 1$ ,  $\Omega_y = 1$ ,  $\gamma_{x,y} = 0.02$ .

Then the reflection coefficients can be obtained through a transfer matrix of the twisted system. In addition, the formalism used to describe the optical properties can be also used for other twisted hyperbolic metasurfaces [54]. Here, the effective conductivity of each single twisted metasurface layer can be obtained considering a twist angle  $\varphi$  along the main axis as

$$\hat{\sigma}_{\varphi} = \begin{pmatrix} \sigma_x & 0 \\ 0 & \sigma_y \end{pmatrix}_{\varphi} = \begin{pmatrix} \sigma_{pp} & \sigma_{ps} \\ \sigma_{sp} & \sigma_{ss} \end{pmatrix}. \quad (14)$$

The twist between the metasurface and the main axis leads to the nondiagonal response  $\sigma_{ps,sp}$ , which is not a result of the intrinsic chirality or magnetism of the plasmonic metasurface. Details about the components of the effective conductivity and transfer matrix below are demonstrated in the Appendix. With the effective conductivity of each twisted metasurface layer derived above, the transfer matrix that connects the electric fields of the first layer with the electric fields of the  $N$ th layer can be obtained from the boundary conditions as

$$\begin{pmatrix} E_{p1}^+ \\ E_{p1}^- \\ E_{s1}^+ \\ E_{s1}^- \end{pmatrix} = \begin{pmatrix} T_{11} & T_{12} & T_{13} & T_{14} \\ T_{21} & T_{22} & T_{23} & T_{24} \\ T_{31} & T_{32} & T_{33} & T_{34} \\ T_{41} & T_{42} & T_{43} & T_{44} \end{pmatrix} \begin{pmatrix} E_{pN}^+ \\ E_{pN}^- \\ E_{sN}^+ \\ E_{sN}^- \end{pmatrix}. \quad (15)$$

The detailed expressions of the effective conductivity and transfer matrix are demonstrated in the Appendix. Therefore, the reflection coefficients can be expressed in terms of the

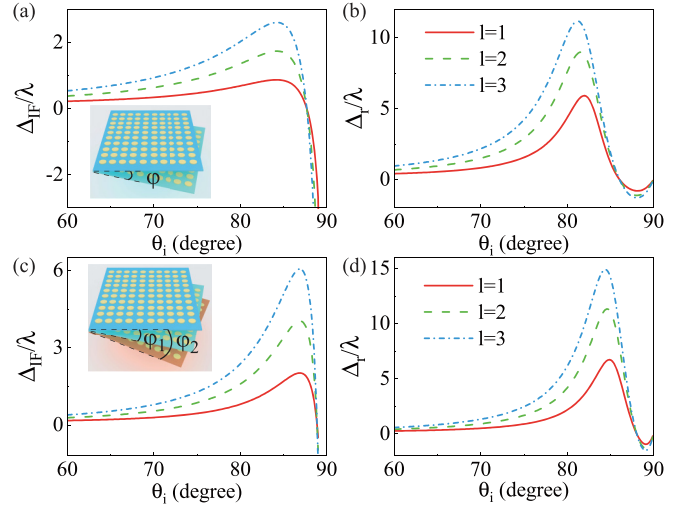


FIG. 2. (a)  $\Delta_{IF}$  of twisted bilayer metasurfaces versus the incident angle. The inset shows the twisted bilayer metasurfaces and the definition of twist angle. (b)  $\Delta_r$  of twisted bilayer metasurfaces versus the incident angle. (c)  $\Delta_{IF}$  of twisted trilayer metasurfaces versus the incident angle. The inset shows the twisted trilayer metasurfaces and the definition of the two twist angles. (d)  $\Delta_r$  of twisted trilayer metasurfaces versus the incident angle. The topological charge is set as  $l = 1, 2, 3$ , respectively. The frequency is set as  $\omega = 1.2$ , with twist angle  $\varphi = 30^\circ$ ,  $\varphi_1 = 30^\circ$ , and  $\varphi_2 = 60^\circ$ .

transfer matrix elements as [53,55,56]

$$\begin{aligned} r_{pp} &= \frac{T_{21}T_{33} - T_{23}T_{31}}{T_{11}T_{33} - T_{13}T_{31}}, & r_{ps} &= \frac{T_{41}T_{33} - T_{43}T_{31}}{T_{11}T_{33} - T_{13}T_{31}}, \\ r_{sp} &= \frac{T_{11}T_{23} - T_{13}T_{21}}{T_{11}T_{33} - T_{13}T_{31}}, & r_{ss} &= \frac{T_{11}T_{43} - T_{13}T_{41}}{T_{11}T_{33} - T_{13}T_{31}}. \end{aligned} \quad (16)$$

### III. RESULTS AND DISCUSSION

Now we consider the spatial IF shift and the PSHE shift on the twisted metasurfaces in two different conditions, in which the twisted bilayer and trilayer metasurfaces are taken into consideration, respectively. Since the thickness of the interlayer between different metasurface layers we consider is large enough, the interaction between the adjacent layer is ignored. The insets in Figs. 2(a) and 2(c) illustrate a clear view of the structure of the twist angle for twisted bilayer and trilayer metasurfaces. For the twisted bilayer metasurfaces, the twist angle is determined as the angle between the respective  $x$  axes of the adjacent metasurface layer. As for the twisted trilayer metasurfaces, the twist angle is determined as the angle between the twisted layer and the first layer. Here the twist angle for twisted trilayer metasurfaces is set as  $\varphi_2 = 2\varphi_1$ .

Figures 2(a) and 2(c) demonstrate the relationship between the incident angle and the spatial IF shift  $\Delta_{IF}$  for the  $p$ -polarized incident vortex beam. The influence of another degree of freedom, that is, the topological charge  $l$  is also shown. Figures 2(b) and 2(d) show the total shift  $\Delta_r$  dependence on the incident angle as well as the topological charge for the  $p$ -polarized incident vortex beam. The results show that the shifts are in the wavelength scale and have a clear dependence on the incident angle as well as the topological

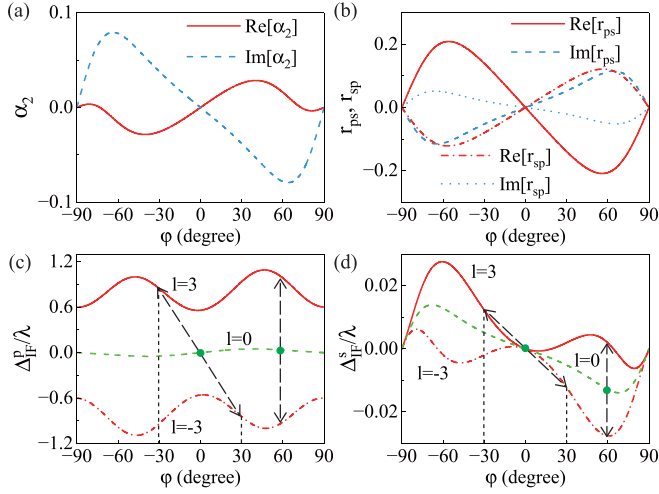


FIG. 3. (a) Real and imaginary parts of parameter  $\alpha_2$  versus twist angle. (b) Real and imaginary parts of reflection coefficients  $r_{ps}$  and  $r_{sp}$ . (c) Spatial IF shifts of twisted bilayer metasurfaces versus the twist angle for  $p$ -polarized beam and topological charge  $l = 0, \pm 3$ . (d) Spatial IF shifts of twisted bilayer metasurfaces versus the twist angle for  $s$ -polarized beam and topological charge  $l = 0, \pm 3$ .

charge. With the change of incident angle, the shifts show similar evolution for different numbers of layers of the twisted metasurface. Although the dependence on the incident angle can be observed for any incident angle, a better view is offered in the range  $60^\circ < \theta_i < 90^\circ$ .

For the fixed twist angle  $\varphi = 30^\circ$  in twisted bilayer metasurfaces and  $\varphi_1 = 30^\circ$  in twisted trilayer metasurfaces,  $\Delta_r$  shifts have maximum value with the incident angle increasing, where the frequency is  $\omega = 1.2$ . Although for different topological charges the amplitude of the shifts differ from each other, they contain similar evolution trends. It can be observed from the figures that the shifts are slightly enhanced when the topological charge increases from  $l = 1$  to  $l = 3$ . In the condition of twisted trilayer metasurfaces and  $l = 3$ , the maximum  $\Delta_r$  can reach the value of  $15\lambda$ . The total shift that is one order of magnitude larger than the wavelength of incident light that can be observed in a narrow range of incident angle, which approaches the true Brewster angle of the twisted metasurfaces.

In Fig. 3 we show the spatial IF shifts of twisted bilayer metasurfaces in a fixed incident angle  $\theta_i = 70^\circ$  and frequency  $\omega = 1.2$  for different topological charge and varying twist angle from  $-90^\circ$  to  $90^\circ$ . In addition, the parameters related to the shifts are shown for the analysis of the symmetry property of the shifts. As an important part of the spin-orbit interaction, spatial IF shift has unique properties when considered in a twisted metasurface system.

Figures 3(c) and 3(d) show that the spatial IF shifts of both incident polarization states are symmetrical about the  $l = 0$  shifts for opposite topological charge in a fixed twist angle, which can be expressed as

$$\begin{aligned} \Delta_{\text{IF}}(\varphi, l = c) - \Delta_{\text{IF}}(\varphi, l = 0), \\ = \Delta_{\text{IF}}(\varphi, l = 0) - \Delta_{\text{IF}}(\varphi, l = -c). \end{aligned} \quad (17)$$

Here  $c$  is a constant and  $c \neq 0$ . This symmetry property is consistent with previous works with proper adjustment [26]. It can be observed that the IF shifts for  $p$ -polarized show slight differences when the metasurface is twisted in different directions, which results from the OAM of the incident beam. Although not shown in the figures, the total shifts  $\Delta_r$  have a similar symmetry property to the IF shifts, which can be expressed as

$$\begin{aligned} \Delta_r(\varphi, l = c) - \Delta_r(\varphi, l = 0) \\ = \Delta_r(\varphi, l = 0) - \Delta_r(\varphi, l = -c). \end{aligned} \quad (18)$$

Since the spatial IF shift vanishes when the twist angle is 0 and the topological charge is 0, the spatial IF shifts of opposite twist angle and opposite topological charge are symmetrical about the origin, that is,

$$\Delta_{\text{IF}}(\varphi, l) = -\Delta_{\text{IF}}(-\varphi, -l). \quad (19)$$

This symmetry property can be predicted from the parameter  $\alpha_2$  as shown in Fig. 3(a), in which the real and imaginary parts of  $\alpha_2$  are symmetrical about the origin. In addition, the symmetry may originate from the reflection coefficients as shown in Fig. 3(b) and the effective conductivities that are not shown here.

The minus sign in Eq. (19) in front of  $\Delta_{\text{IF}}$  on the right side represents the shift is in a different direction. Considering the symmetry is relative to the  $l = 0$  shifts, changing the sign of the topological charge only changes the direction of the shifts relatively. Since changing the sign of the twist angle only affects the value of the shifts, this leaves the direction of the shifts relatively unchanged. This results in the minus sign in Eq. (19). Although the symmetry can be expanded to arbitrary opposite topological charges, only the condition of  $l = \pm 3$  is demonstrated in Fig. 3. It provides a good method for the identification and modulation of the twist angle and the topological charge.

In spite of the topological charge and twist angle, frequency is also a key factor of the interaction between the vortex beam and twisted metasurfaces. The PSHE shifts of the right-circular polarized beam for different frequency are presented in Figs. 4(a) and 4(b). Here, the solid line refers to  $l = 3$  and the point dashed line refers to  $l = -3$ . With the frequency increasing, the variation of the shifts becomes flatter. For a better view of the symmetry of the PSHE shifts, the frequency is set as  $\omega = 1.2$  in Figs. 4(c) and 4(d). Different from the spatial IF shifts, the PSHE shifts are only symmetrical about the  $l = 0$  shift. Although the shifts of the  $p$ -polarized beam and  $s$ -polarized beam differ in the amplitude and variation trend, the symmetry property is consistent.

Next we turn our attention to another factor that also plays a role in the spin-orbit interaction of twisted light and twisted metasurfaces. When the layer of the twisted metasurfaces is increased to 3 and more, the twist structure can be pretty complicated with different twist angle combinations. Here, we only expand it to the trilayer system for a simple but clear enough demonstration of the impact of the twist structure. Figure 5 plots the dependence of the spatial IF shifts and PSHE shifts of twisted trilayer metasurfaces with the twist angles  $\varphi_1$  and  $\varphi_2$  of the system.

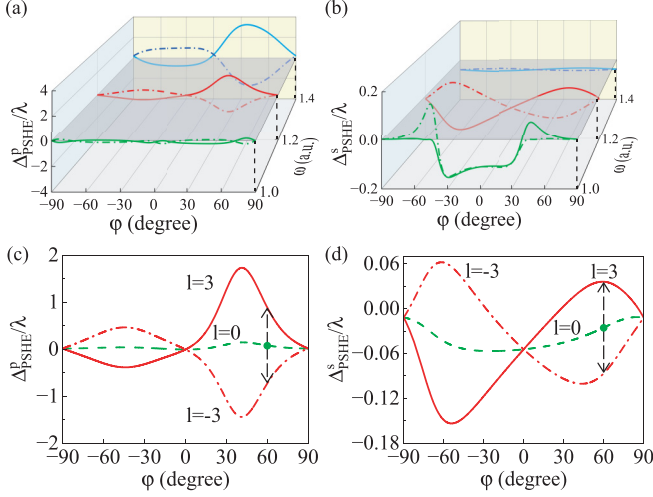


FIG. 4. (a), (b) PSHE shifts of twisted bilayer metasurfaces versus the twist angle for  $p$ -polarized and  $s$ -polarized incident beams, respectively. Here the solid lines refer to topological charge  $l = 3$  and point dashed lines refer to topological charge  $l = -3$ . The frequency is  $\omega = 1.0, 1.2, 1.4$ . (c), (d) PSHE shifts of twisted bilayer metasurfaces versus the twist angle for  $p$ -polarized and  $s$ -polarized incident beams, respectively. Here the topological charge is  $l = 0, \pm 3$  and frequency  $\omega = 1.2$ .

It could be noticed that specific twist structures can give rise to maximum or minimum value of the spatial IF shifts and the PSHE shifts. That means the shifts can be easily controlled by just adjusting the structure of the twisted metasurfaces without changing any other parameters. The multiple combinations of the twist angles and different dependence of the shifts on the twisted metasurfaces make the spatial IF shift and the PSHE shift more flexible. Combined with each other, the spatial IF shift and PSHE shift have full information of the twist angle, which means the twist angle can be measured from the shifts. Although it is hard for one to obtain a simple-enough expression for the twist angle using the IF shifts and

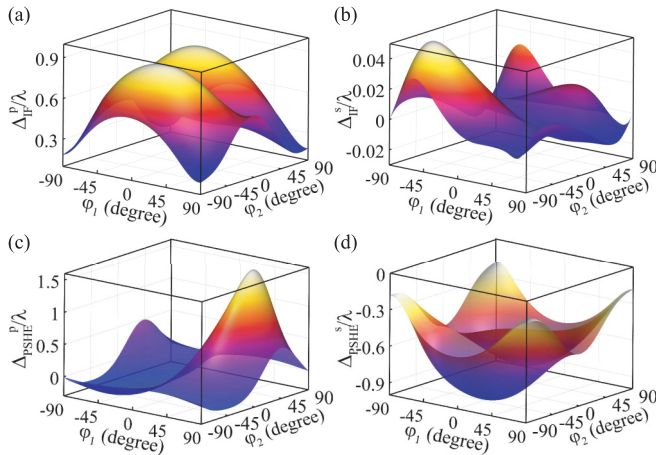


FIG. 5. (a), (b) Spatial IF shifts of twisted trilayer metasurfaces dependence with the twist angles  $\varphi_1$  and  $\varphi_2$ . (c), (d) PSHE shifts of twisted trilayer metasurfaces dependence with the twist angles  $\varphi_1$  and  $\varphi_2$ . The topological charge is set as  $l = 3$ .

PSHE shifts, the shifts enables a complete determination of the twist structure of the twisted metasurfaces.

#### IV. CONCLUSION

In conclusion, we investigated the spin-orbit interaction between the vortex beam and twisted hyperbolic metasurfaces with bilayer and trilayer structures. By deriving the reflection field of the incident vortex beam on the twisted metasurfaces via the angular spectrum method, we demonstrated the spatial IF shift and PSHE shift of twisted light interacting with twisted metasurfaces. The resulting shifts are in the wavelength scale and carry clear fingerprints of the twisted metasurface structure, which show a clear symmetry property with the twist angle and topological charge. Our results show that the twist properties of light and metasurfaces can be a good tool for the metrology of each other.

#### ACKNOWLEDGMENTS

This work was supported by the National Natural Science Foundation of China (Grant No. 12174097) and the Natural Science Foundation of Hunan Province (Grant No. 2021JJ10008).

#### APPENDIX: EFFETIVE CONDUCTIVITY AND TRANSFER MATRIX

Here we derive the effective conductivity of the twisted metasurfaces and the transfer matrix. The conductivity of a monolayer metasurface that consists of a 2D uniaxial plasmonic array is demonstrated in Eqs. (12) and (13). Therefore, for a twisted metasurface layer with twist angle  $\varphi$  along the main axis, the effective conductivity can be obtained through coordinate transformation as

$$\begin{aligned} \hat{\sigma}_\varphi &= \begin{pmatrix} \sigma_{pp} & \sigma_{ps} \\ \sigma_{sp} & \sigma_{ss} \end{pmatrix} \\ &= \begin{pmatrix} \cos \varphi & -\sin \varphi \\ \sin \varphi & \cos \varphi \end{pmatrix} \begin{pmatrix} \sigma_x & 0 \\ 0 & \sigma_y \end{pmatrix} \begin{pmatrix} \cos \varphi & \sin \varphi \\ -\sin \varphi & \cos \varphi \end{pmatrix}, \end{aligned}$$

with

$$\begin{aligned} \sigma_{pp} &= \sigma_x \cos^2 \varphi + \sigma_y \sin^2 \varphi, \\ \sigma_{ps} &= (\sigma_y - \sigma_x) \cos \varphi \sin \varphi, \\ \sigma_{sp} &= (\sigma_y - \sigma_x) \cos \varphi \sin \varphi, \\ \sigma_{ss} &= \sigma_x \sin^2 \varphi + \sigma_y \cos^2 \varphi. \end{aligned} \quad (\text{A1})$$

The effective conductivity of the twisted second layer or third layer metasurface can be then obtained according to the twist angle.

With the effective conductivity of each layer, the transfer matrix for the adjacent layer of the twisted metasurfaces can be obtained through the boundary conditions. The boundary conditions on the twisted metasurfaces for both the  $p$ -polarized and  $s$ -polarized beams can be expressed as

$$E_{s1}^+ + E_{s1}^- = E_{s2}^+ + E_{s2}^-, \quad (\text{A2})$$

$$(E_{p1}^+ + E_{p1}^-) \cos \theta_1 = (E_{p2}^+ + E_{p2}^-) \cos \theta_2, \quad (\text{A3})$$

$$\frac{1}{Z_1}(E_{p1}^+ + E_{p1}^-) = (\sigma_{pp}E_{p2}^+ \cos \theta_2 + \sigma_{ps}E_{s2}^+) + \frac{1}{Z_2}(E_{p2}^+ + E_{p2}^-), \quad (\text{A4})$$

$$\frac{1}{Z_1}(E_{s1}^+ - E_{s1}^-) \cos \theta_1 = (\sigma_{ss}E_{s2}^+ + \sigma_{sp}E_{p2}^+) + \frac{1}{Z_2}(E_{s2}^+ - E_{s2}^-) \cos \theta_2. \quad (\text{A5})$$

Here,  $\theta_j$  is the incident angle in the corresponding medium and  $Z_j$  is the impedance of the medium. Through solving the boundary conditions the transfer matrix can be obtained as

$$\begin{pmatrix} E_{p1}^+ \\ E_{p1}^- \\ E_{s1}^+ \\ E_{s1}^- \end{pmatrix} = T_{1,2} \begin{pmatrix} E_{p2}^+ \\ E_{p2}^- \\ E_{s2}^+ \\ E_{s2}^- \end{pmatrix}, \quad (\text{A6})$$

with

$$T_{1,2} = \frac{1}{2} \begin{bmatrix} \frac{Z_1}{Z_2} \begin{pmatrix} a_1^+ & a_2^- \\ a_1^- & a_2^+ \end{pmatrix} & Z_1 \sigma_{ps} \begin{pmatrix} 1 & 0 \\ 1 & 0 \end{pmatrix} \\ \cos \theta_2 Z_1 \sigma_{sp} \begin{pmatrix} 1 & 0 \\ -1 & 0 \end{pmatrix} & \frac{Z_1}{Z_2} \begin{pmatrix} b_1^+ & b_2^- \\ b_1^- & b_2^+ \end{pmatrix} \end{bmatrix},$$

$$a_1^\pm = 1 \pm \frac{\cos \theta_2 Z_2}{\cos \theta_1 Z_1} + \cos \theta_2 Z_2 \sigma_{pp},$$

$$a_2^\pm = 1 \pm \frac{\cos \theta_2 Z_2}{\cos \theta_1 Z_1},$$

$$b_1^\pm = \pm \cos \theta_2 + \frac{Z_2}{Z_1} \pm Z_2 \sigma_{ss},$$

$$b_2^\pm = \pm \cos \theta_2 + \frac{Z_2}{Z_1}. \quad (\text{A7})$$

Then the transfer matrix can be easily expanded to an arbitrary number of layers by multiplying the transfer matrix that connects each other as

$$T_{1 \rightarrow N+1} = T_{1 \rightarrow 2} T_{d_1} T_{2 \rightarrow 3} T_{d_{N-1}} T_{N \rightarrow N+1}, \quad (\text{A8})$$

with

$$T_{d_j} = \begin{pmatrix} e^{-ik_{zj}d_j} & 0 & 0 & 0 \\ 0 & e^{ik_{zj}d_j} & 0 & 0 \\ 0 & 0 & e^{-ik_{zj}d_j} & 0 \\ 0 & 0 & 0 & e^{ik_{zj}d_j} \end{pmatrix}. \quad (\text{A9})$$

Here, the factor  $T_{j \rightarrow j+1}$  can be obtained from  $T_{1 \rightarrow 2}$  by replacing the refractive index and the effective conductivity. The total transfer matrix of a twisted  $N$  layers system, as shown in Eq. (15), can be obtained with effective conductivity from the above formula.

- 
- [1] L. Allen, M. W. Beijersbergen, R. J. C. Spreeuw, and J. P. Woerdman, Orbital angular momentum of light and the transformation of Laguerre-Gaussian laser modes, *Phys. Rev. A* **45**, 8185 (1992).
- [2] G. Molina-Terriza, J. P. Torres, and L. Torner, Twisted photons, *Nat. Phys.* **3**, 305 (2007).
- [3] B. J. McMorran, A. Agrawal, I. M. Anderson, A. A. Herzing, H. J. Lezec, J. J. McClelland, and J. Unguris, Electron vortex beams with high quanta of orbital angular momentum, *Science* **331**, 192 (2011).
- [4] C. E. M. Demore, Z. Yang, A. Volovick, S. Cochran, M. P. MacDonald, and G. C. Spalding, Mechanical Evidence of the Orbital Angular Momentum to Energy Ratio of Vortex Beams, *Phys. Rev. Lett.* **108**, 194301 (2012).
- [5] A. Anhäuser, R. Wunenburger, and E. Brasselet, Acoustic Rotational Manipulation Using Orbital Angular Momentum Transfer, *Phys. Rev. Lett.* **109**, 034301 (2012).
- [6] K. Y. Bliokh and F. Nori, Transverse and longitudinal angular momenta of light, *Phys. Rep.* **592**, 1 (2015).
- [7] K. Bliokh, I. Ivanov, G. Guzzinati, L. Clark, R. Van Boxem, A. Béché, R. Juchtmans, M. Alonso, P. Schattschneider, F. Nori, and J. Verbeeck, Theory and applications of free-electron vortex states, *Phys. Rep.* **690**, 1 (2017).
- [8] H. Tong, G. Xie, Z. Qiao, Z. Qin, P. Yuan, J. Ma, and L. Qian, Generation of a mid-infrared femtosecond vortex beam from an optical parametric oscillator, *Opt. Lett.* **45**, 989 (2020).
- [9] Q. Zhao, M. Dong, Y. Bai, and Y. Yang, Measuring high orbital angular momentum of vortex beams with an improved multi-point interferometer, *Photon. Res.* **8**, 745 (2020).
- [10] L. Xu, D. Li, J. Chang, D. Li, T. Xi, and Z. Hao, Powerful supercontinuum vortices generated by femtosecond vortex beams with thin plates, *Photon. Res.* **10**, 802 (2022).
- [11] M. J. Padgett and L. Allen, Orbital angular momentum exchange in cylindrical-lens mode converters, *J. Opt. B: Quantum Semiclassical Opt.* **4**, S17 (2002).
- [12] A. S. Ostrovsky, C. Rickenstorff-Parrao, and V. Arrizón, Generation of the “perfect” optical vortex using a liquid-crystal spatial light modulator, *Opt. Lett.* **38**, 534 (2013).
- [13] X. Yi, X. Ling, Z. Zhang, Y. Li, X. Zhou, Y. Liu, S. Chen, H. Luo, and S. Wen, Generation of cylindrical vector vortex beams by two cascaded metasurfaces, *Opt. Express* **22**, 17207 (2014).
- [14] S. Chen, X. Zhou, Y. Liu, X. Ling, H. Luo, and S. Wen, Generation of arbitrary cylindrical vector beams on the higher order poincaré sphere, *Opt. Lett.* **39**, 5274 (2014).
- [15] H. Wang, L. Liu, C. Zhou, J. Xu, M. Zhang, S. Teng, and Y. Cai, Vortex beam generation with variable topological charge based on a spiral slit, *Nanophotonics* **8**, 317 (2019).
- [16] S. M. A. Hosseini-Saber, E. A. Akhlaghi, and A. Saber, Diffractometry-based vortex beams fractional topological charge measurement, *Opt. Lett.* **45**, 3478 (2020).
- [17] A. M. Yao and M. J. Padgett, Orbital angular momentum: Origins, behavior and applications, *Adv. Opt. Photon.* **3**, 161 (2011).
- [18] M. Duocastella and C. Arnold, Bessel and annular beams for materials processing, *Laser Photonics Rev.* **6**, 607 (2012).
- [19] J. Zhou, Y. Liu, Y. Ke, H. Luo, and S. Wen, Generation of Airy vortex and Airy vector beams based on the modulation of dynamic and geometric phases, *Opt. Lett.* **40**, 3193 (2015).

- [20] Z. Liu, Y. Liu, Y. Ke, Y. Liu, W. Shu, H. Luo, and S. Wen, Generation of arbitrary vector vortex beams on hybrid-order poincaré sphere, *Photon. Res.* **5**, 15 (2017).
- [21] Y. Liu, Y. Ke, J. Zhou, Y. Liu, H. Luo, S. Wen, and D. Fan, Generation of perfect vortex and vector beams based on Pancharatnam-Berry phase elements, *Sci. Rep.* **7**, 44096 (2017).
- [22] M. Merano, N. Hermosa, J. P. Woerdman, and A. Aiello, How orbital angular momentum affects beam shifts in optical reflection, *Phys. Rev. A* **82**, 023817 (2010).
- [23] W. Long, J. Pan, X. Guo, X. Liu, H. Lin, H. Zheng, J. Yu, H. Guan, H. Lu, Y. Zhong, S. Fu, L. Zhang, W. Zhu, and Z. Chen, Optimized weak measurement of orbital angular momentum-induced beam shifts in optical reflection, *Photon. Res.* **7**, 1273 (2019).
- [24] K. Y. Bliokh, M. A. Alonso, E. A. Ostrovskaya, and A. Aiello, Angular momenta and spin-orbit interaction of nonparaxial light in free space, *Phys. Rev. A* **82**, 063825 (2010).
- [25] K. Y. Bliokh, I. V. Shadrivov, and Y. S. Kivshar, Goos-hänchen and Imbert-Fedorov shifts of polarized vortex beams, *Opt. Lett.* **34**, 389 (2009).
- [26] Z. Xiao, H. Luo, and S. Wen, Goos-Hänchen and Imbert-Fedorov shifts of vortex beams at air-left-handed-material interfaces, *Phys. Rev. A* **85**, 053822 (2012).
- [27] L. Zhuo, W. Long, M. Jiang, W. Zhu, H. Guan, J. Tang, J. Yu, H. Lu, J. Zhang, and Z. Chen, Graphene-based tunable Imbert-Fedorov shifts and orbital angular momentum sidebands for reflected vortex beams in the terahertz region, *Opt. Lett.* **43**, 2823 (2018).
- [28] A. Aiello, N. Lindlein, C. Marquardt, and G. Leuchs, Transverse Angular Momentum and Geometric Spin Hall Effect of Light, *Phys. Rev. Lett.* **103**, 100401 (2009).
- [29] Y. Zhang, P. Li, S. Liu, and J. Zhao, Unveiling the photonic spin Hall effect of freely propagating fan-shaped cylindrical vector vortex beams, *Opt. Lett.* **40**, 4444 (2015).
- [30] X. Ling, X. Yi, X. Zhou, Y. Liu, W. Shu, H. Luo, and S. Wen, Realization of tunable spin-dependent splitting in intrinsic photonic spin Hall effect, *Appl. Phys. Lett.* **105**, 151101 (2014).
- [31] M. P. J. Lavery, S. M. Barnett, F. C. Speirits, and M. J. Padgett, Observation of the rotational Doppler shift of a white-light, orbital-angular-momentum-carrying beam backscattered from a rotating body, *Optica* **1**, 1 (2014).
- [32] M. Zhao, X. Gao, M. Xie, W. Zhai, W. Xu, S. Huang, and W. Gu, Measurement of the rotational doppler frequency shift of a spinning object using a radio frequency orbital angular momentum beam, *Opt. Lett.* **41**, 2549 (2016).
- [33] T. A. Fadeyeva, A. F. Rubass, and A. V. Volyar, Transverse shift of a high-order paraxial vortex-beam induced by a homogeneous anisotropic medium, *Phys. Rev. A* **79**, 053815 (2009).
- [34] W. Zhu, M. Jiang, H. Guan, J. Yu, H. Lu, J. Zhang, and Z. Chen, Tunable spin splitting of Laguerre-Gaussian beams in graphene metamaterials, *Photon. Res.* **5**, 684 (2017).
- [35] S. Carr, D. Massatt, S. Fang, P. Cazeaux, M. Luskun, and E. Kaxiras, Twistronics: Manipulating the electronic properties of two-dimensional layered structures through their twist angle, *Phys. Rev. B* **95**, 075420 (2017).
- [36] S. Zhao, L. Shao, J. Wang, H.-Q. Lin, and W. Zhang, Chirality-selective transparency induced by lattice resonance in bilayer metasurfaces, *Photon. Res.* **9**, 484 (2021).
- [37] K. Khaliji, L. Martín-Moreno, P. Avouris, S.-H. Oh, and T. Low, Twisted Two-Dimensional Material Stacks for Polarization Optics, *Phys. Rev. Lett.* **128**, 193902 (2022).
- [38] D. Kang, Z.-W. Zuo, Z. Wang, and W. Ju, Bandgap engineering of stacked two-dimensional polyaniline by twist angle, *Appl. Phys. Lett.* **119**, 061602 (2021).
- [39] W. J. M. Kort-Kamp, F. J. Culchac, R. B. Capaz, and F. A. Pinheiro, Photonic spin Hall effect in bilayer graphene moiré superlattices, *Phys. Rev. B* **98**, 195431 (2018).
- [40] N. Yu and F. Capasso, Flat optics with designer metasurfaces, *Nat. Mater.* **13**, 139 (2014).
- [41] C.-J. Kim, A. Sánchez-Castillo, Z. Ziegler, Y. Ogawa, C. Noguez, and J. Park, Chiral atomically thin films, *Nat. Nanotechnol.* **11**, 520 (2016).
- [42] G. Hu, A. Krasnok, Y. Mazor, C.-W. Qiu, and A. Alù, Moiré hyperbolic metasurfaces, *Nano Lett.* **20**, 3217 (2020).
- [43] H. Herzig Sheinfux and F. H. L. Koppens, The rise of twist-optics, *Nano Lett.* **20**, 6935 (2020).
- [44] G. Hu, C.-W. Qiu, and A. Alù, Twistronics for photons: Opinion, *Opt. Mater. Express* **11**, 1377 (2021).
- [45] J. Zhou, S. Liu, H. Qian, Y. Li, H. Luo, S. Wen, Z. Zhou, G. Guo, B. Shi, and Z. Liu, Metasurface enabled quantum edge detection, *Sci. Adv.* **6**, eabc4385 (2020).
- [46] J. Zhou, H. Qian, C.-F. Chen, J. Zhao, G. Li, Q. Wu, H. Luo, S. Wen, and Z. Liu, Optical edge detection based on high-efficiency dielectric metasurface, *Proc. Natl. Acad. Sci. USA* **116**, 11137 (2019).
- [47] S. He, R. Wang, and H. Luo, Computing metasurfaces for all-optical image processing: A brief review, *Nanophotonics* **11**, 1083 (2022).
- [48] D. Xu, H. Yang, W. Xu, W. Zhang, K. Zeng, and H. Luo, Inverse design of Pancharatnam-Berry phase metasurfaces for all-optical image edge detection, *Appl. Phys. Lett.* **120**, 241101 (2022).
- [49] Z. Li, W. Liu, H. Cheng, J. Liu, S. Chen, and J. Tian, Simultaneous generation of high-efficiency broadband asymmetric anomalous refraction and reflection waves with few-layer anisotropic metasurface, *Sci. Rep.* **6**, 35485 (2016).
- [50] J. Duan, N. Capote-Robayna, J. Taboada-Gutiérrez, G. Álvarez-Pérez, I. Prieto, J. Martín-Sánchez, A. Y. Nikitin, and P. Alonso-González, Twisted nano-optics: Manipulating light at the nanoscale with twisted phonon polaritonic slabs, *Nano Lett.* **20**, 5323 (2020).
- [51] Y. Liu, C. Ouyang, Q. Xu, X. Su, Q. Yang, J. Ma, Y. Li, Z. Tian, J. Gu, L. Liu, J. Han, Y. Shi, and W. Zhang, Moiré-driven electromagnetic responses and magic angles in a sandwiched hyperbolic metasurface, *Photon. Res.* **10**, 2056 (2022).
- [52] W. Zhang, W. Wu, S. Chen, J. Zhang, X. Ling, W. Shu, H. Luo, and S. Wen, Photonic spin Hall effect on the surface of anisotropic two-dimensional atomic crystals, *Photon. Res.* **6**, 511 (2018).
- [53] O. V. Kotov and Y. E. Lozovik, Hyperbolic hybrid waves and optical topological transitions in few-layer anisotropic metasurfaces, *Phys. Rev. B* **100**, 165424 (2019).
- [54] A. Girich, L. Ivzhenko, A. Hrinchenko, S. Tarapov, and O. Yermakov, Manipulation over surface waves in bilayer hyperbolic metasurfaces: Topological transition and multidirectional

- canalization, *IEEE Microw. and Wireless Tech. Lett.* **33**, 367 (2022).
- [55] P. Yeh, Electromagnetic propagation in birefringent layered media, *J. Opt. Soc. Am.* **69**, 742 (1979).
- [56] W. Zhang, Y. Wang, S. Chen, S. Wen, and H. Luo, Photonic spin Hall effect in twisted few-layer anisotropic two-dimensional atomic crystals, *Phys. Rev. A* **105**, 043507 (2022).